



저작자표시-비영리-변경금지 2.0 대한민국

이용자는 아래의 조건을 따르는 경우에 한하여 자유롭게

- 이 저작물을 복제, 배포, 전송, 전시, 공연 및 방송할 수 있습니다.

다음과 같은 조건을 따라야 합니다:



저작자표시. 귀하는 원저작자를 표시하여야 합니다.



비영리. 귀하는 이 저작물을 영리 목적으로 이용할 수 없습니다.



변경금지. 귀하는 이 저작물을 개작, 변형 또는 가공할 수 없습니다.

- 귀하는, 이 저작물의 재이용이나 배포의 경우, 이 저작물에 적용된 이용허락조건을 명확하게 나타내어야 합니다.
- 저작권자로부터 별도의 허가를 받으면 이러한 조건들은 적용되지 않습니다.

저작권법에 따른 이용자의 권리는 위의 내용에 의하여 영향을 받지 않습니다.

이것은 [이용허락규약\(Legal Code\)](#)을 이해하기 쉽게 요약한 것입니다.

[Disclaimer](#)

Thesis for the Degree of Master of Science

**Seismic Activity in the  
Pyeongnam Basin Area of the  
Korean Peninsula**

The logo of Pukyong National University is a circular emblem. It features a central stylized design with a blue and grey color scheme, possibly representing a globe or a specific symbol. The words "PUKYONG NATIONAL UNIVERSITY" are written in a circular path around the inner edge of the emblem. Below the emblem, the Korean text "부경대학교" is visible.

by

Heekyoung Lee

Division of Earth Environmental System Science

The Graduate School

Pukyong National University

February 2017

Seismic Activity in the  
Pyeongnam Basin Area of the  
Korean Peninsula  
(한반도 평남분지의 지진활동)

Advisor: Prof. Tae-Seob Kang

by

Heekyoung Lee

A thesis submitted in partial fulfillment of the requirements  
for the degree of

Master of Science

in Division of Earth Environmental Science,  
The Graduate school,  
Pukyong National University

February 2017

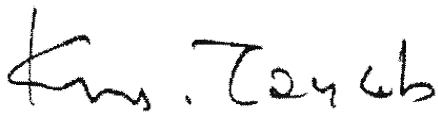
Seismic Activity in the Pyeongnam Basin Area  
of the Korean Peninsula

A dissertation  
by  
Heekyoung Lee

Approved by:



(Chairman) Young-Seog Kim



(Member) Tae-Seob Kang



(Member) Ho Seon Choi

February 24, 2017

# CONTENTS

|   |           |
|---|-----------|
| List of Figures .....                           | iii       |
| List of Tables .....                            | vii       |
| Abstract .....                                  | viii      |
| <b>I . Introduction .....</b>                   | <b>1</b>  |
| 1.1 Background .....                            | 1         |
| 1.2 Geology .....                               | 4         |
| <b>II . Stations and Data Preparation .....</b> | <b>10</b> |
| <b>III . Method .....</b>                       | <b>13</b> |
| 3.1 Relocation .....                            | 13        |
| 3.2 Focal mechanism .....                       | 17        |

|                         |    |
|-------------------------|----|
| 3.3 Stress field .....  | 24 |
| 3.4 Rose diagram .....  | 26 |
| IV. Discussion .....    | 27 |
| V. Conclusions .....    | 29 |
| References .....        | 31 |
| Appendix .....          | 43 |
| Summary in Korean ..... | 46 |

## List of Figures

**Fig 1.** Seismicity in and around the Korean Peninsula since the launch of the instrument seismological observatory in 1978. Epicenters are marked based on the list from KMA and KIGAM. The size of the circle refers to the magnitude and the blue square box represents the research area. ....7

**Fig 2.** The brown lines highlight major tectonic structures of the Korean Peninsula (from Hong(2010)). HFB (the Hambuk fold belt), GMB (Gilju- Myeongcheon basin), NM (the Nangnim massif), PB (the Pyeongnam basin), OB (the Ongjin basin), IFB (the Imjingang fold belt), GM (the Gyeongsang massif), OFB (the Okcheon fold belt), YM (the Yeongnam massif), GB (the Gyeongsang Basin), HUB (the Hupo bank and basin), and YIB (the Yeonil basin). ....8

**Fig 3.** Geological map (1:1,000,000) of the Hwanghae Province (KIGAM, 1995). The legend is shown at the upper left corner. The rock type and the geological structure are classified by colors. The line on the map marks the fault. ....9

**Fig 4.** Location of the KMA and KIGAM seismic stations used in this study. Most broad-band seismic stations and some short-period stations are used. The red triangle indicates the KMA network and the blue square represents the KIGAM network. ....11

**Fig 5.** The waveform of the earthquake event that occurred on March 14, 2016. This figure shows P and S arrival time at each station. The used stations are YPDB, DACB, SEO2, SHHB, SNU, GAPB, and HWCB. ....12

**Fig 6.** (a) The focal depth of the determined epicenters at each event. The x-axis and y-axis correspond to each event with numbers and determined depths, respectively. Symbol '+' (in black) is the depth values in the KIGAM data; symbol 'x' (in red) means the depth values determined in the present study. (b) The cross sections with latitude and longitude. ....15

**Fig 7.** Focal mechanisms of 27 earthquakes. Most events seem to be oblique faults with normal components. The background seismicity is marked with the open blue circle. The focal mechanism in the orange color represents the event that occurred on February 14, 1982. The epicentral

location and magnitude of the event were taken from the ISC catalog; focal depth was obtained from the literature. ....21

**Fig 8.** 3D focal mechanisms and the cross-sectional view. (a) Topography with the range of the research area is used and the focal mechanisms are put at the determined depths under the surface. The arrow shows a northward direction. Most events seem to be oblique strike-slip faults with normal components. (b) The range of research area (38.5°N~38.9°N, 125.6°E~126.3°E) is marked by  $\overline{XX^1}$  line in the cross section. The average depth is determined as 11.56km and most of the determined hypocenter depths are constrained within a somewhat narrow zone(depth<16km). ....22

**Fig 9.** Triangle diagram (Frohlich, 1992) for plotting 27 focal mechanisms. The graph shows similarity and diversity of earthquake focal mechanisms. Three peaks correspond to the reverse fault, normal fault, and strike-slip fault, respectively. None of these criteria were defined as 'odd' mechanisms combining two or three focal mechanism components. For some events, the calculated values were different, but they were overlaid at the same position. ....23

**Fig 10.** Principal stress axis directions calculated from 27 focal mechanisms.  $\overline{XX'}$  is marked due to the different geology settings on the boundary. Two types of dominant directions are the ENE-WSW and WNW-ESE. The event that occurred on March. 14, 2016 is presented at the upper right of the corner. The focal mechanism and stress axis direction of horizontally projected P-axis are also plotted. ....25

**Fig 11.** Rose diagram with the trend of P axis calculated from 27 focal mechanisms. Each bar represents the direction of the lineament and the bar length means the frequency. (a) The trend directions of P axes calculated from a total of 27 events, (b) the lower region of the  $\overline{XX'}$  boundary is shown as the NE-SW direction, and (c) the NW-SE direction is dominant in the upper region of the  $\overline{XX'}$  boundary. ....26

**Appendix A.** Focal mechanism solutions of 27 events. ....43

## List of Tables

|   |    |
|---|----|
| <b>Table 1.</b> Source parameters of the 33 earthquakes from KMA and KIGAM catalogs.....  | 35 |
| <b>Table 2.</b> Relocated hypocenters of 33 events in this study....  | 38 |
| <b>Table 3.</b> Parameters of fault plane solutions for 27 earthquakes that are analyzed using the seismic polarity analysis..... | 41 |

Seismic Activity in the Pyeongnam Basin Area of  
the Korean Peninsula

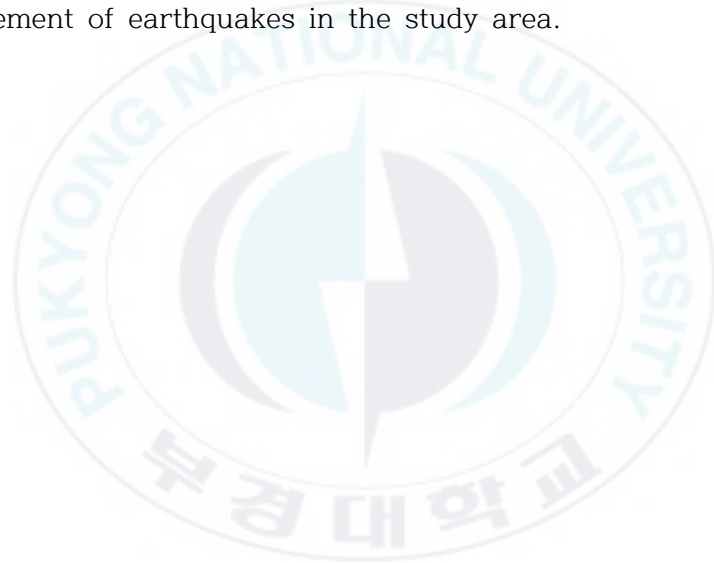
Heekyoung Lee

Division of Earth Environmental System Science, The Graduate School,  
Pukyong National University

**Abstract**

The northwestern part of the Korean Peninsula geologically belongs to the Pyeongnam Basin. The study area shows a comparatively higher seismicity, as compared to the rest of the northern part of the Korean Peninsula where seismicity is somewhat lower than in the southern part; however, there are historical records of large earthquakes in the research area. A representative example is a moderate earthquake that occurred at Sariwon, North Hwanghae Province, on February 14, 1982. In this study, a total of 33 earthquakes of magnitudes above 2.0 that had occurred between March 2008 and August 2016 were analyzed. Due to the lack of direct seismic observation, an iterative optimal solution technique for minimizing the travel time residuals was used with an algorithm to search for the optimum velocity model. Most of the determined depths were constrained within a somewhat narrow zone ranging from about 10 km to 15 km. The focal mechanism solutions of 27 earthquakes were obtained from the P-wave first

motion polarities. The results indicate that some events were associated with the faulting motions' combination of strike-slip and normal senses, and of which the trends of the pressure axes were in the ENE-WSW and WNW-ESE directions. This may imply that the stress field in the area was locally perturbed, but the background physics remains uncertain. Background seismicity, source parameters, focal mechanism solutions, and the stress field analysis are expected to be helpful for a better understanding of the characteristics and fault movement of earthquakes in the study area.



# I . Introduction

## 1.1 Background

Earthquakes on the Korean Peninsula, which belong to the intra-plate region, show a relatively low seismicity, small magnitude, and typically irregular epicenter location, as compared to inter-plate earthquakes (Kim et al., 2006). In the case of large-scale earthquakes, even if the distance is considerable, the energy is sufficiently strong to be analyzed and the waveform quality of the seismic wave is good. However, the earthquakes that occur in and around the Korean Peninsula are typically small to moderate-sized, so the data from the domestic seismic network can be obtained. The analysis of small to medium-sized earthquakes helps not only to identify seismic source parameters, but also to understand the mechanism of occurrence of earthquakes and tectonic settings. Therefore, it is important to continuously analyze earthquakes and accumulate seismic data.

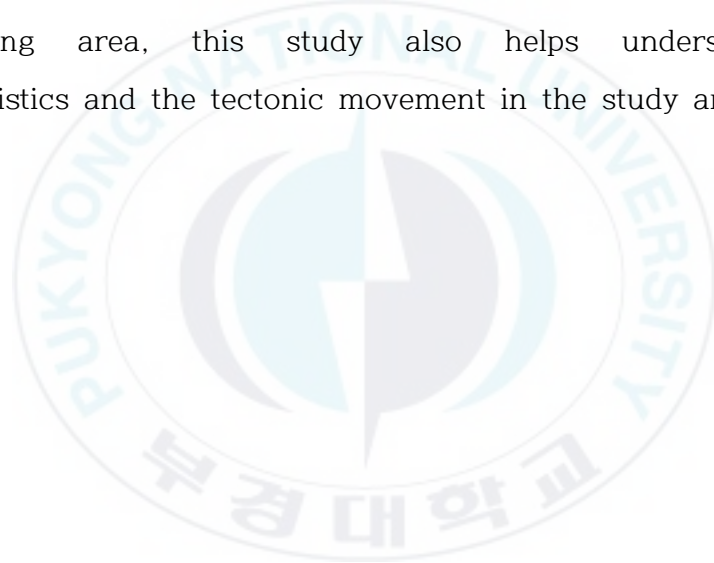
A dense seismic network is required for a reliable seismic analysis. As a result of a larger than normal earthquake in the Hongsung area in 1978, Korea realized the need for a seismic network of its own, and began to build an analog seismic network. In 1997, a digital network was launched. Many earthquake

researchers have analyzed seismic activity in and around the Korean Peninsula (Jun, 1991; Kim et al., 2006; Park et al., 2007; Jun and Jeon, 2010; Rhie and Kim, 2010; Hong and Choi, 2012; Kyung et al., 2001; Jung and Kyung, 2013; Lee et al., 2014). However, the history of the earthquake research remains too short. Moreover, our knowledge of the geology of the north part of the Korean Peninsula mostly depends on the literature and there are many difficulties in explaining the formation process and the tectonic structure of the Korean Peninsula.

In previous research on the fault plane solution, the earthquakes that occurred in and around the Korean Peninsula were mostly characterized by dominantly strike-slip faulting with partly thrust components (Kim et al., 2006; Jun and Jeon, 2010). The average P-axis is nearly horizontal to the ENE-WSW or NE-SW direction. However, there are not many studies in this area and it is difficult to clarify the cause why, according to some researchers (e.g., Kim et al., 2006; Jun, 1991; Rhie and Kim, 2010; Park et al., 2012), the Hwanghae Province shows an unusual pattern.

In this study, a total of 33 earthquakes with the magnitude of 2.0 or higher that occurred in the North Hwanghae Province between March, 2008 and August, 2016 are analyzed. The seismic data were acquired and collected from KMA (Korea Meteorological Administration) and KIGAM (Korea Institute of Geoscience and Mineral Resources). Then, by removing the mean value and gradient component and by making all waveforms have the same

start time, the seismic data were transformed for further analysis. In order to minimize the error of the recorded seismic travel time at each station, the location of the epicenters was re-determined by using an iterative algorithm. With the FOCMEC (FOCAL MECHANISM determination) method, the fault plane solutions were obtained to analyze the mechanism of fault movement. By comparing the direction of the main stress causing the earthquake with the regional stress direction in the Korean Peninsula and the surrounding area, this study also helps understand the characteristics and the tectonic movement in the study area.



## 1.2 Geology

After the Hongsung earthquake occurred in 1978, an analogue earthquake monitoring system was built and the observation of earthquakes became possible in the south part of the Korean Peninsula. Since the seismic data of the early 20th century are similar to those of historical earthquakes, the location of the epicenters is not specified in detail. There is a considerable difference in accuracy and reliability is somewhat low. In addition, North Korea's Earthquake Research Institute produced a catalog of historical earthquakes during the period A.D. 2 - 1983. However, since a document was written by a person, there is a high possibility of omissions, exaggerations, and typing errors (Kim et al., 2006).

Among the province of the northern part of the Korean Peninsula, the North Hwanghae Province shows a particularly high seismicity and small-sized earthquakes have constantly occurred in this area. Fig. 1 shows the epicentral distribution in and around the Korean Peninsula since the launch of the instrument seismological observatory in 1978. Seismicity in the northern part of the Korean Peninsula is somewhat low as compared to the southern part of the peninsula, but there is a historical record of large earthquakes. A representative example is a medium-scale earthquake ( $M_b=5.1$  and

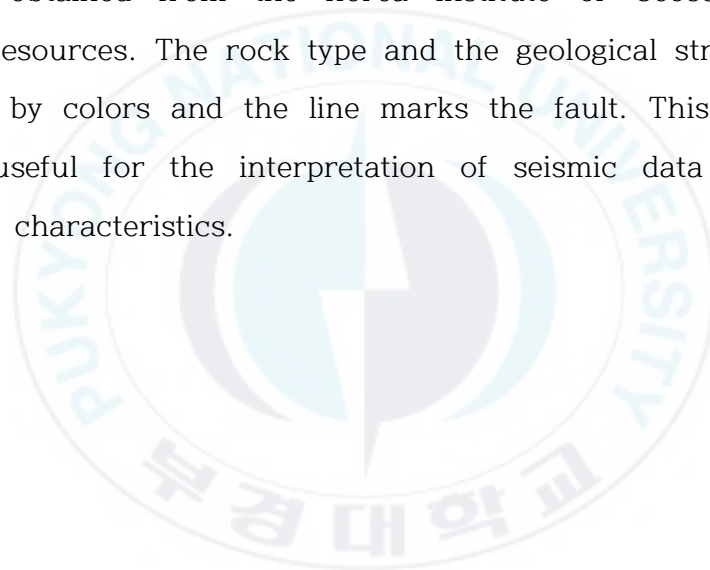
$M_s=5.2$  from Jun (1991)) that occurred at Sariwon, the North Hwanghae Province, on February 14, 1982. This study area corresponds to the Pyeongnam basin, which is the boundary between the Nangnim massif and the Gyeonggi massif (see Fig. 2). According to *Geology of Korea* (1996), the Pyeongnam basin has a deep geological history as the sedimentary basin formed on the fold. The continental crust showed an originally different tectonic setting between the north and south, with the line connecting the boundary of the Hwangju-Koksan-Anbyon. Post sediments of the Sangwon system are bounded by a thin layer of sedimentary layers in the northern part of the boundary and the entire sequences of the Sangwon system are developed in the south. The southern region of the massif was created at a very rapid rate during the middle-late Proterozoic era, while the sedimentary rocks formed in the northern part subsided later and slowly. Geological layers differ one from another due to a difference in the speed of sedimentation.

The Pyeongnam basin is composed of the Archean-Lower Proterozoic basement group, the Sangwon-Hwangju system, and the Pyongan system. The Mesozoic and Cenozoic graben-type basins partially overlap. The sedimentary layers affected by the Songnim disturbance after the Pyongan system were deposited. Afterwards, the sedimentary layers were influenced by fold, thrust fault movement, metamorphism, and magma intrusion.

In the case of the fault structures developed in the Pyeongnam

basin, the faults with the NWW strike from the Ryesonggang fault developed in the western part and the NNE strike is dominant in the eastern part. In addition, the faults in the NE and NW directions have been extensively developed within the basin under the influence of the Taebo and Jaeryonggang tectonic movement (*Geology of Korea*, 1996).

Fig. 3 shows the geological map (1:1,000,000) of the Hwanghae Province obtained from the Korea Institute of Geoscience and Mineral Resources. The rock type and the geological structure are classified by colors and the line marks the fault. This geological map is useful for the interpretation of seismic data based on geological characteristics.



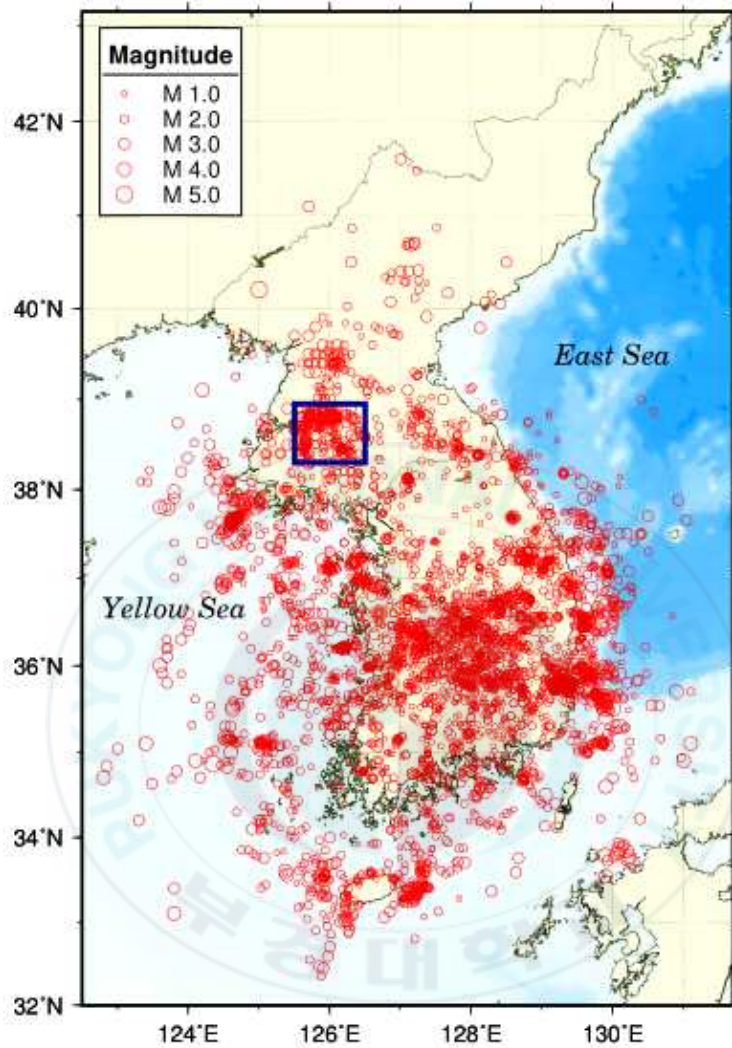


Fig. 1. Seismicity in and around the Korean Peninsula since the launch of the instrument seismological observatory in 1978. Epicenters are marked based on the list from KMA and KIGAM. The size of the circle refers to the magnitude and the blue square box represents the research area.

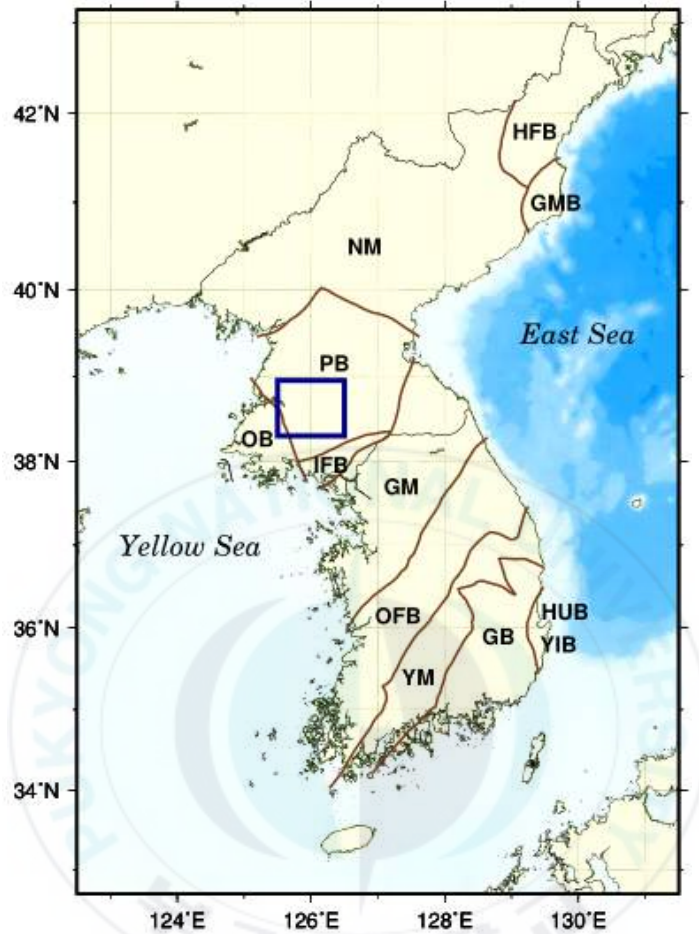


Fig. 2. The brown lines highlight major tectonic structures of the Korean Peninsula (from Hong(2010)). HFB (the Hambuk fold belt), GMB (Gilju- Myeongcheon basin), NM (the Nangnim massif), PB (the Pyeongnam basin), OB (the Ongjin basin), IFB (the Imjingang fold belt), GM (the Gyeongsang massif), OFB (the Okcheon fold belt), YM (the Yeongnam massif), GB (the Gyeongsang Basin), HUB (the Hupo bank and basin), and YIB (the Yeonil basin).

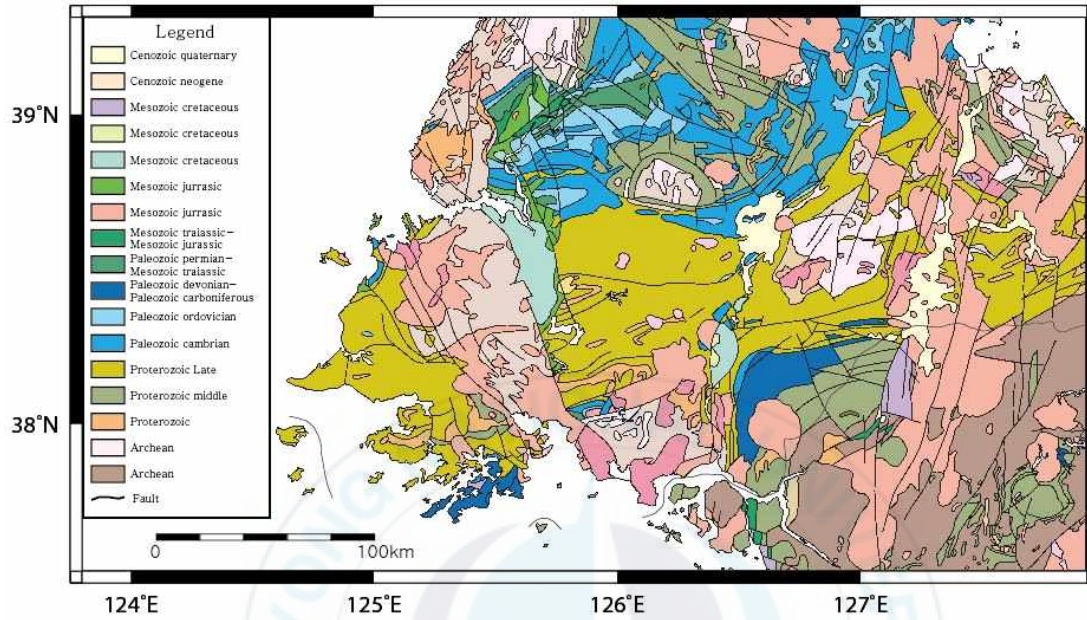


Fig. 3. Geological map (1:1,000,000) of the Hwanghae Province (KIGAM, 1995). The legend is shown at the upper left corner. The rock type and the geological structure are classified by colors. The line on the map marks the fault.

## II. Stations and Data Preparation

Overall, 40 earthquakes with the magnitude of 2.0 or higher occurred in the northern Hwanghae Province from March 2008 to August 2016. The number of earthquakes is 16 in the Songrim area, 11 in Sariwon, 8 in Pyongsan, and 5 in Singye. For some events, the quality of the data was poor. As the distance increases from the epicenter, it is difficult to accurately distinguish the signals from the noise and the RMS value also increases. Therefore, 33 of 40 earthquakes have been analyzed for relocation.

The seismic data were obtained from KMA and KIGAM. After converting the file of MiniSEED, a form of raw data, into the SAC file format that can analyze the waveform, the average value and the gradient component were removed and the start time of all waveforms was set to be identical. In this study, due to the risk of a damage of the waveform data, a specific band pass filter was not used. Since the number of broadband observation stations capable of detecting both local earthquakes and teleseismic is gradually increasing and it is distributed densely and evenly, seismic data were analyzed using most broadband stations and some short-period station data. The location and distribution of the stations used in this study are shown in Fig. 4. Fig. 5 shows the seismic waveform data of the earthquake that occurred on March 14, 2016. It indicates the arrival time of the P and S waves at each station near the epicenter.

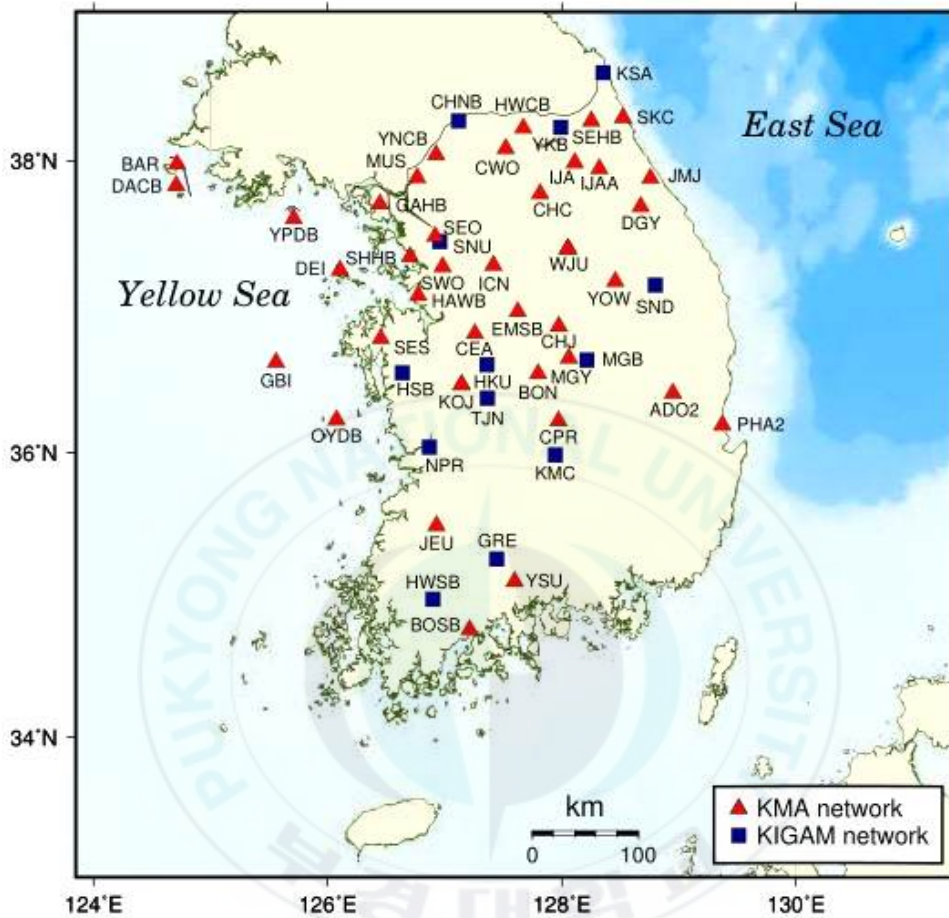


Fig. 4. Location of the KMA and KIGAM seismic stations used in this study. Most broad-band seismic stations and some short-period stations are used. The red triangle indicates the KMA network and the blue square represents the KIGAM network.

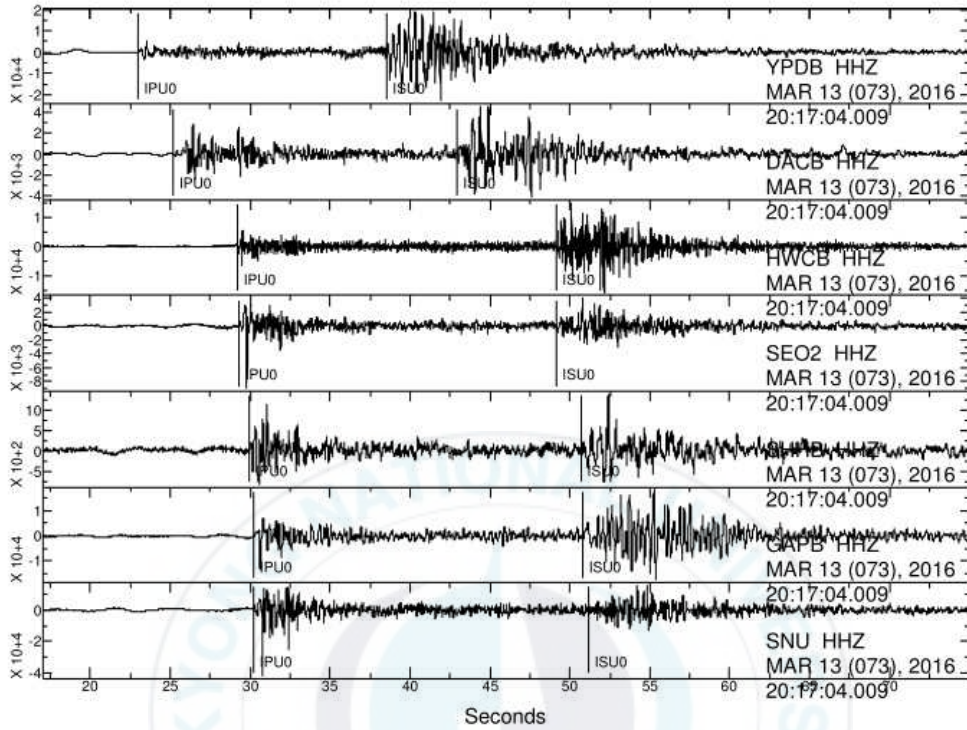


Fig. 5. The waveform of the earthquake event that occurred on March 14, 2016. This figure shows P and S arrival time at each station. The used stations are YPDB, DACB, SEO2, SHHB, SNU, GAPB, and HWCB.

## III. Method

### 3.1 Relocation

Analyzing the source parameters is the most basic yet important step in understanding the characteristics of earthquakes. Source parameters include information on the origin time, the epicenter (latitude and longitude), and the focal depth. The accuracy is determined by the waveform of good quality, station distribution, crustal velocity model, and the inversion algorithm (Kim et al., 2014).

In this study, a program referred to as VELELLIPSE (Kim, 2014), which is a combination of HYPOELLIPSE (Lahr, 1980) with the proposed algorithm, was applied to determine the epicenters, focal depth, and origin time of the earthquakes. HYPOELLIPSE, one of the conventional methods, calculates hypocentral parameters based on given velocity models. However, VELELLIPSE finds the optimal one-dimensional velocity structure model for hypocentral inversions with the algorithm, iteratively searching for the best-fitting average velocity model. As compared to conventional methods, this method shows an improved computational accuracy. Therefore, it is useful in the areas where the exact velocity structure is not known, such as the North Korea region. The

method unfolds as follows.

A suitable P-wave and S-wave velocity models are determined and a P-wave velocity model that moves at a constant velocity in the initial P-wave velocity model is prepared (see Eq. (1)).

$$\alpha_i^n = \alpha_i^0 + n\Delta\alpha, \alpha_s^n = \alpha_s^0 + n\Delta\alpha, \quad (1)$$

where  $\Delta\alpha$  : constant velocity interval

$n$  : integer from 0 to N

$\alpha_i^0$  : P-wave velocity in the  $i$ th layer of the initial velocity model

$\alpha_i^n$  : P-wave velocity in the  $i$ th layer of the  $n$ th velocity model

The number of velocity models is represented as N + 1. For each velocity model, the synthetic travel time of the P and S waves is calculated, followed by the calculation of the misfit error between the synthetic and the observed travel time. The misfit error, F, can be obtained from the following equation (see Eq. (2)):

$$F = \frac{\sqrt{3\overline{\Delta t_p^2} + \overline{\Delta t_s^2}}}{4}, \quad (2)$$

where  $\overline{\Delta t_p}$  : travel time differences of P wave

$\overline{\Delta t_s}$  : travel time differences of S wave

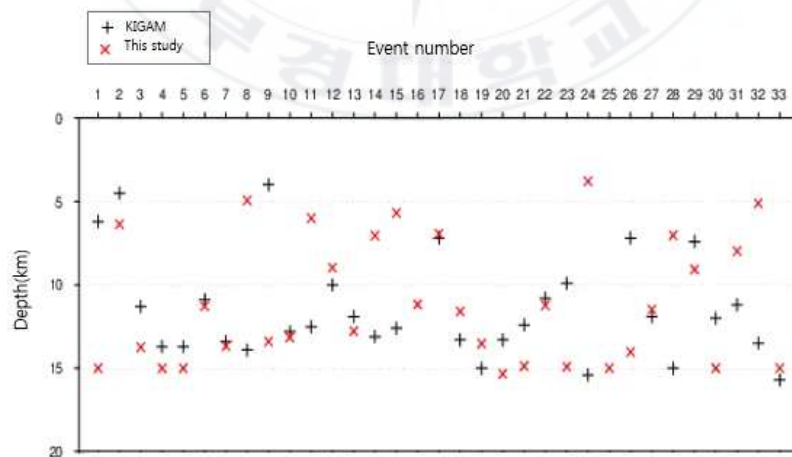
The determined velocity model can be used as an initial reference velocity model to implement a more advanced model in Eq. (1). It can be repeatedly calculated until the misfit error obtains a minimum value. The final optimal velocity model is obtained from

the velocity model with the minimum misfit error (Kim et al., 2014).

Based on the lists released by KMA and KIGAM, the information on source parameters is shown in Table 1 and the relocated parameters are reported in Table 2. Fig. 6 shows the determined depth of epicenters by KIGAM and the results of the present study, respectively. Although the location of the epicenters suggested by our results seems to be similar the KMA results, the straight distance ranges from 10 km to 15 km. In the case of the origin time, the maximum difference was 2.439 seconds (No. 32). Except for the event (No. 25), the average focal depth was determined as 11.56 km.

The reason for the difference in the analysis results is the differences in the program used at each institution, crust velocity structure model, initial arrival time, and seismic stations.

(a)



(b)

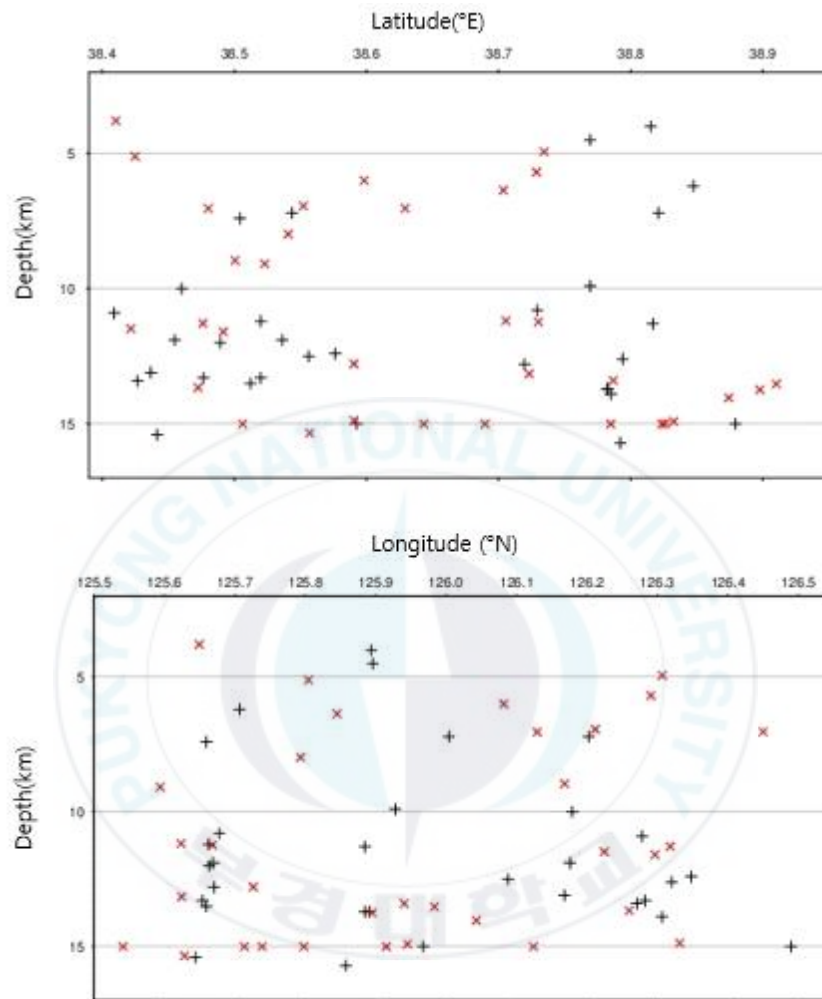


**Fig. 6.** (a) The focal depth of the determined epicenters at each event. The x-axis and y-axis correspond to each event with numbers and determined depths, respectively. Symbol '+' (in black) is the depth values in the KIGAM data; symbol 'x' (in red) means the depth values determined in the present study. (b) The cross sections with latitude and longitude.

## 3.2 Focal mechanism

The polarity of the waveform was picked manually from the seismic data where it would be comparatively easy to distinguish the signal from the noise. The fault plane solutions were analyzed with FOCMEC (Snoke, 2000) based on the re-determined source parameters. When the number of fault plane solutions was large, the median value was selected. The 1D crustal velocity structure model (Chang and Baag, 2006) was used for the focal mechanism determination. This is the most commonly used model and it does not have a large standard deviation by region, as compared to the other southern crustal velocity structure models. This model is based on the algorithms for the receiver function and surface wave dispersion obtained from a teleseismic recorded at 22 broadband stations in the southern part of the Korean Peninsula from 1999 to 2003 (Kim et al., 2006).

In this study, the azimuth coverage was not good, because the seismic data located in the southern part of the Korean Peninsula were analyzed. Most earthquakes are small to medium-sized earthquakes with the magnitude of  $2 \leq M < 4$ ; thus, picking the accurate signal from the noise was not always certain. Thus, for a comparatively optimal focal mechanism determination, 27 of 33 re-determined events were analyzed using as much seismic data around the epicenter as possible. The seismic data used for the analysis vary from 10 to 28 stations.

Fig. 6 shows the analyzed focal mechanisms based on the redetermined epicentral locations. Various components of the mechanism can be seen. The open blue circle shows seismic activity based on the list from KMA. The focal mechanism, shown with the orange color, is the medium-sized earthquake ( $M_b = 5.1$ ,  $M_s = 5.2$ ) that occurred in the Sariwon area on February 14, 1982. The epicentral location and the magnitude were taken from the catalog by International Seismological Center (ISC); the focal depth was taken from the analysis results reported by Jun(1991). The hypocentral location was determined as 38.46°N, 125.65°E and the focal depth was 9km. According to the results of the focal mechanism, the earthquake was an oblique normal faulting with a plane of strike 245°, dip 44°, and rake 243°. A total of 27 focal mechanisms are summarized in Table 3 and Appendix A.

The information on aftershock distributions or near fault direction, as well as the strike and dip direction on the fault plane and the auxiliary plane, was combined to determine the fault plane (Jung and Kyung, 2013). According to *Geology of Korea* (1999), the steeply dipping Ryesonggang fault in the NWW direction and the fault in the eastern region with the NNE strike are predominant in the Pyeongnam basin. The faults with the NE and NW directions are widely developed in the basin under the influence of the Taebo and Jaeryonggang tectonic movements. Since a geological survey cannot be conducted in this study area, information on geology and faults has been borrowed from the literature, and it is difficult

to judge whether the result is related to a specific fault due to the lack of data.

Fig. 7 represents 3D focal mechanisms from the analysis of the focal mechanism using two nodal planes of strike, dip, rake, trend, and plunge of P-axis and T-axis. The topography of the study area (38.5°N to 38.9°N, 125.6°E to 126.3°E) was applied to show the structure on the surface and the angles were varied to show the focal mechanisms in three dimensions. As the fault is not a single line on the surface but a plane, it helps to explain the focal depth and fault motion of the earthquakes.

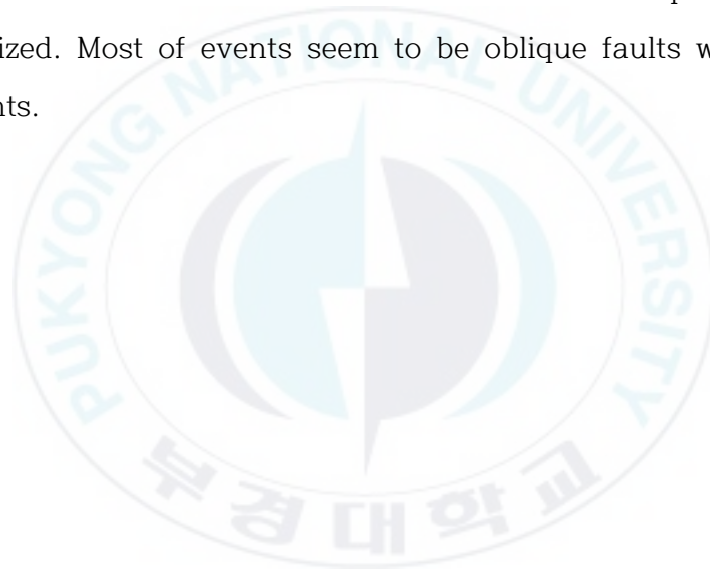
The focal mechanisms are characterized as thrust, strike-slip, and normal faulting by the ternary diagram (Frohlich, 2001) in terms of the dip angles with respect to T, B, and P axes. Similarity and diversity of earthquake focal mechanisms can be seen from the ternary graph. Frohlich and Apperson (1992) classified the type of faulting based on the following equation (see Eq. (3)):

$$\sin^2\delta_T + \sin^2\delta_B + \sin^2\delta_P = 1 \quad (3)$$

where  $\delta_T$ ,  $\delta_B$ , and  $\delta_P$  are the dip angles with respect to T, B, and P axes, respectively. If a dip angle of the B-axis exceeds 60°, the mechanism is defined as the strike-slip faulting. The normal faulting is declared, when a dip angle of the P-axis exceeds 60°; the mechanism is regarded as thrust faulting when a dip angle of T-axis is greater than 50°. Mechanisms belonging to none of these criteria are defined as 'odd' mechanisms that combine two or three

focal mechanism components.

Fig. 8 shows a triangle diagram of the focal mechanism solutions for 27 earthquakes. Three peaks correspond to the reverse fault, normal fault, and strike-slip fault, respectively. For some events, the calculated values were different, but they were overlaid at the same position in the ternary graph. Two events show normal faults (No. 9 and 22) and No. 10 and 17 belong to strike-slip faults. The strike-slip faults with normal or thrust components are characterized. Most of events seem to be oblique faults with normal components.



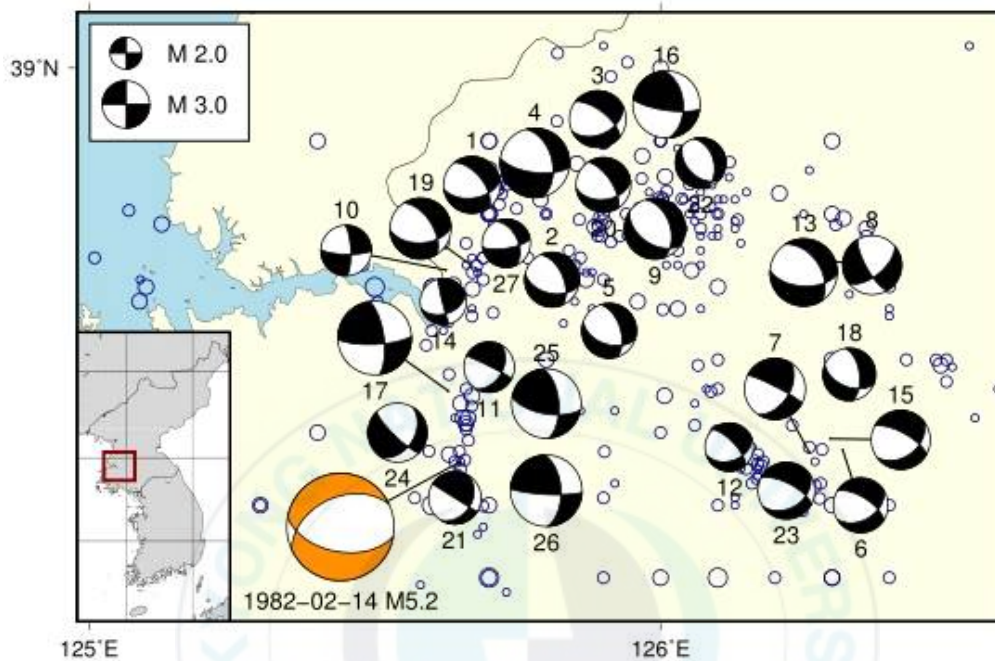
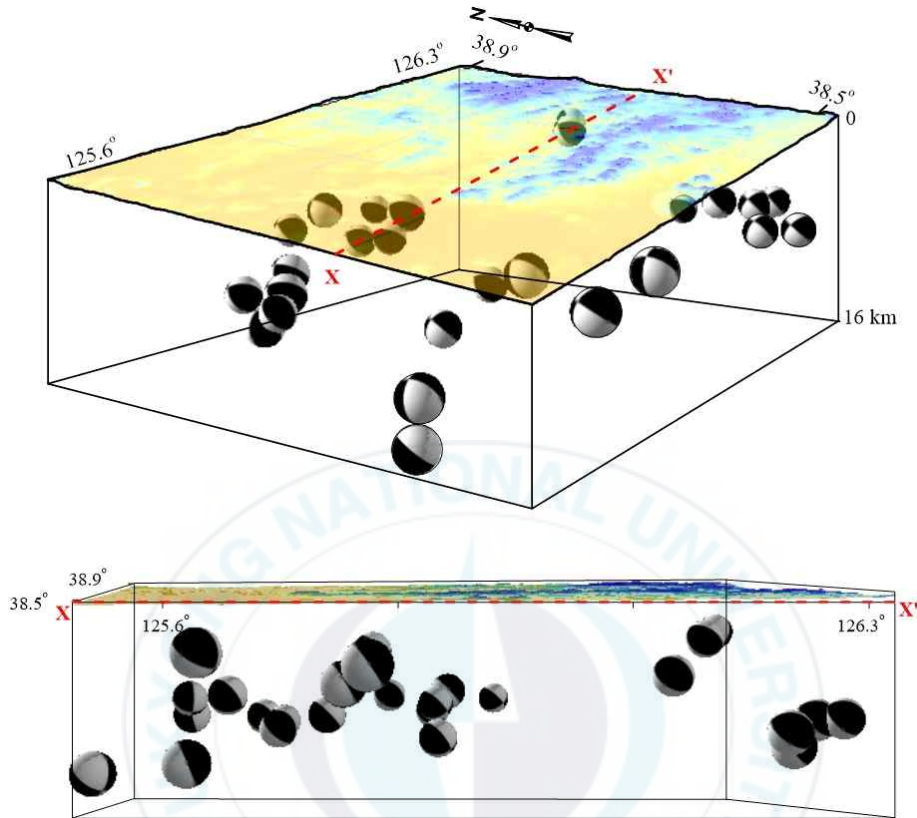


Fig. 7. Focal mechanisms of 27 earthquakes. Most events seem to be oblique faults with normal components. The background seismicity is marked with the open blue circle. The focal mechanism in the orange color represents the event that occurred on February 14, 1982. The epicentral location and magnitude of the event were taken from the ISC catalog; focal depth was obtained from the literature.



**Fig. 8.** 3D focal mechanisms and the cross-sectional view. (a) Topography with the range of the research area is used and the focal mechanisms are put at the determined depths under the surface. The arrow shows a northward direction. Most events seem to be oblique strike-slip faults with normal components. (b) The range of research area ( $38.5^\circ\text{N}\sim 38.9^\circ\text{N}$ ,  $125.6^\circ\text{E}\sim 126.3^\circ\text{E}$ ) is marked by  $\overline{XX'}$  line in the cross section. The average depth is determined as 11.56km and most of the determined hypocenter depths are constrained within a somewhat narrow zone (depth<16km).

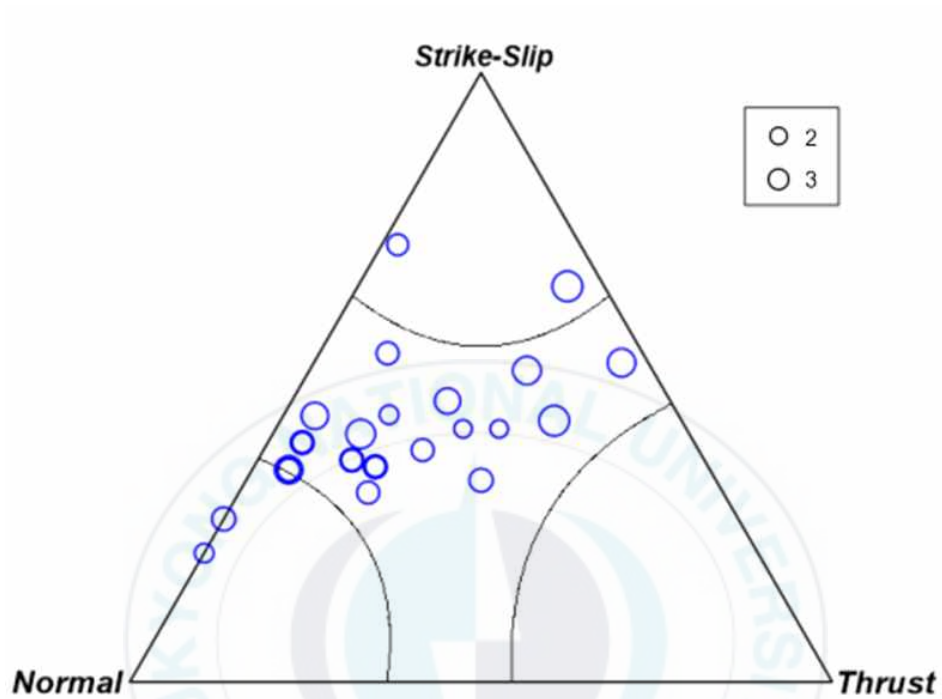


Fig. 9. Triangle diagram (Frohlich, 1992) for plotting 27 focal mechanisms. The graph shows similarity and diversity of earthquake focal mechanisms. Three peaks correspond to the reverse fault, normal fault, and strike-slip fault, respectively. None of these criteria were defined as 'odd' mechanisms combining two or three focal mechanism components. For some events, the calculated values were different, but they were overlaid at the same position.

### 3.3 Stress field

Analyzing the fault plane solutions can explain not only the characteristics of the fault motion, but also the principal stress directions. Fig. 9 shows the directions of the compressional stresses from P-axes calculated for each event. 10 earthquakes (No. 7, 8, 11, 15, 16, 17, 21, 24, 25, and 26) were represented in the NE-SW direction and the orientation of some events (No. 3, 6, and 23) was seen as ENE-WSW. This is similar to the primary stress field in the southern part of the Korean Peninsula. However, 9 fault planes (No. 2, 4, 5, 9, 10, 13, 18, 22, and 27) were laid in the NW-SE directions and 5 fault planes were showed in the WSW-ESE directions. As an example, the focal mechanism and stress axis direction of horizontally projected P-axis were presented at the upper right of Fig. 9. The earthquake with the magnitude of 3.1 occurred in the Songrim area on March 14, 2016. The event was characterized as an oblique strike-slip fault with normal components in the NW-SE directional compression.  $\overline{XX}$  is marked due to the different geology settings at the boundary.

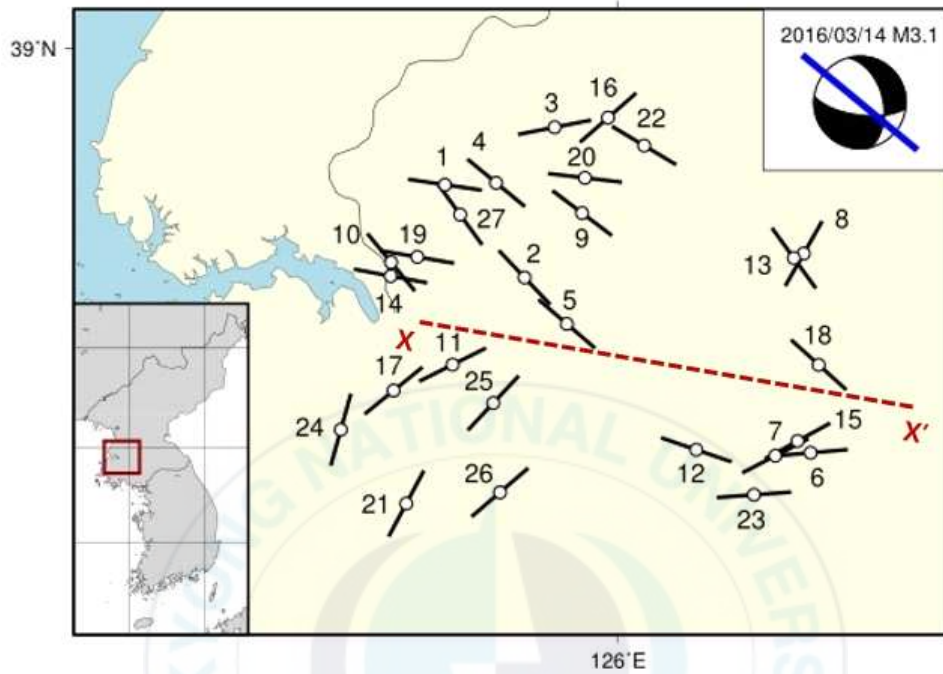
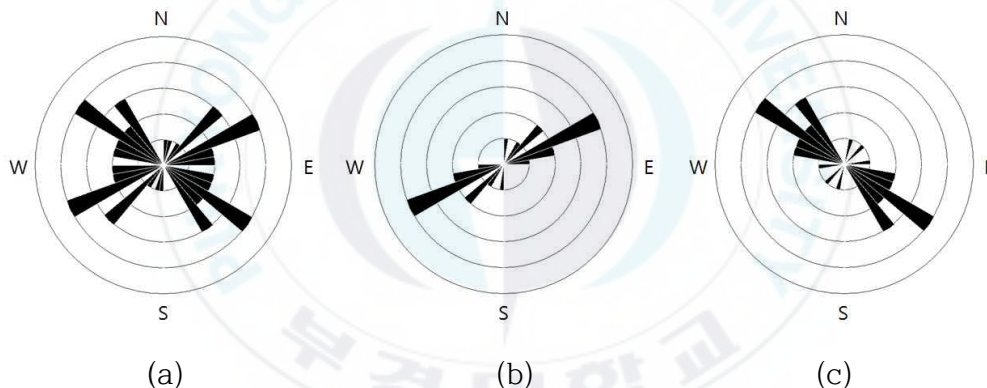


Fig. 10. Principal stress axis directions calculated from 27 focal mechanisms.  $\overline{XX}$  is marked due to the different geology settings on the boundary. Two types of dominant directions are the ENE-WSW and WNW-ESE. The event that occurred on March. 14, 2016 is presented at the upper right of the corner. The focal mechanism and stress axis direction of horizontally projected P-axis are also plotted.

### 3.4 Rose diagram

Figure 10 is a rose diagram using the P-axis trend calculated from the focal mechanism analysis. It is used to express the linear structure, such as a columnar joint or a fault line. Each bar represents the direction of the lineament and the length of the bar means the frequency. Two directions were clearly distinguished in the ENE-WSW and ESE-WNW directions.



**Fig. 11.** Rose diagram with the trend of P axis calculated from 27 focal mechanisms. Each bar represents the direction of the lineament and the bar length means the frequency. (a) The trend directions of P axes calculated from a total of 27 events, (b) the lower region of the  $\overline{XX'}$  boundary is shown as the NE-SW direction, and (c) the NW-SE direction is dominant in the upper region of the  $\overline{XX'}$  boundary.

## IV. Discussion

The results of previous studies (Rhie and Kim, 2010; Choi, 2012; Hong and Choi, 2012) show that there are strike-slip faults with normal components in the northwestern part of the Korean Peninsula. Several maximum horizontal stress directions seem to have different values from the regional average value of the Korean Peninsula (Rhie and Kim, 2010). However, it is difficult to prove the cause and effect of these differences in the northwestern part of the study area.

According to Park (2012), a moderate earthquake with the magnitude of 5.3 that occurred in the Yellow Sea on January 12, 2011 shows a strike-slip fault and a low stress drop. If the tectonic condition around the Yellow Sea is different from that of the Korean Peninsula, the mechanism and the characteristics of earthquakes may also be different. The stress drop in the Yellow Sea was significantly lower than that of other regions where medium-scale earthquakes occurred. The lower stress drop and many active aftershocks may create a different structural environment from that of the Korean Peninsula.

According to Choi (2012), a great number of normal faulting earthquakes occurred around the central Yellow Sea and the northern margin of the North China. The cause of this phenomenon is the influence of pull-apart basin formation by

crustal extension, which is related to strike-slip faulting or small-scale mantle upwelling.

The fault plane solutions of micro-earthquakes are strongly influenced by local stress variation or change (Jung and Kyung, 2013) and the P wave polarity method is affected by the distribution of seismic stations (Rhie and Kim, 2010). Thus, the results may differ depending on the program used for the analysis. For a more accurate analysis, it is necessary to reduce the number of fault plane solutions by using the S/P amplitude ratio and use other methods like TDMT so that to compare the results with those reported in previous research. Furthermore, Chinese seismic waveform data can help obtain more accurate and reliable results with a uniform distribution of azimuths.

## V. Conclusions

In this study, we sought to understand the characteristics of earthquakes and fault movements from seismicity, source parameters, fault plane solutions, and stress field analysis. A total of 33 earthquakes with the magnitude of 2.0 or higher that occurred from March 2008 to August 2016 were analyzed. The hypocentral location was determined with the iterative algorithm searching for the optimum velocity structure model. It was repeatedly calculated until the residual time recorded from each station was minimized. A comparison of the KMA data and the results of the study suggests that the location of the epicenter had a difference of up to about 17 km in the straight line distance and the maximum of 2.439 seconds in the case of the origin time (No. 32). Most of the determined depths were constrained within a somewhat narrow zone ranging from 10 km to 15 km. The range of errors varied for each event, with the minimum depth of 0.26km and the maximum depth of 11.61km (except for event No. 25). The determined average focal depth of the epicenters was analyzed to be about 11.56 km. Therefore, the differences in the analysis results may be due to a variety of reasons, such as the program used by each institution, crustal velocity structure model, first arrival time, and seismic stations used for the analysis.

Based on the information of determined 27 source parameters

among 33 events, the focal mechanism was analyzed using the P-wave first polarity method. According to the triangle diagram suggested by Frohlich (1992), some events (No. 9 and 22) showed the characteristics of normal faults, while earthquakes No. 10 and 17 were characterized as strike-slip faults. The rest of the earthquakes were shown as strike-slip faults with normal or thrust components. The odd mechanisms, which belong to none of those criteria, appeared to be dominant in the study area. Most earthquakes were characterized with the oblique features of the strike-slip faults including normal components.

The principal compressional stress axes calculated from a fault plane solution analysis are shown with two kinds of directions: ENE-WSW and ESE-WNW. For the ESE-WNW direction, it is somewhat different from the regional compressive stress direction on the Korean Peninsula. This appears to be a local phenomenon in certain areas and it is difficult to clearly identify the cause.

The rose diagram was used to study the relation with regard to the linear structure in the study area. Two kinds of directions were clearly distinguished: ENE-WSW and ESE-WNW.

## References

- Chang, S.-J., and Baag, C.-E., 2006, Crustal structure in southern Korea from joint analysis of regional broadband waveforms and travel times, *Bulletin of the Seismological Society of America*, **96**, 856-870.
- Cho, H.-K., Kang, T.-S., and Kyung, J.-B., 2006, Focal mechanism solution of microearthquakes in the southwestern part of the Korean Peninsula, *Journal of The Korean Earth Science Society*, **27**, 341-347.
- Choi, H.-S., 2012, Seismic characteristics of earthquakes around the Korean Peninsula and their tectonic implications, *Ph. D. thesis*, Seoul National University, 125 p.
- Frohlich, C., 1992, Triangle diagrams: ternary graphs to display similarity and diversity of earthquake focal mechanisms, *Physics of the Earth and Planetary Interiors*, **75**, 193-198.
- Frohlich, C., and Apperson, K.-D., 1992, Earthquake focal mechanisms, moment tensors, and the consistency of seismic activity near plate boundaries, *Tectonics*, **11**, 297-296.

- Hoe, S.-Y., and Kyung, J.-B., 2008, Fault plane solutions for the recent earthquakes in the central region of South Korea, *Journal of the Korean Earth Science Society*, **29**, 437-445.
- Hong, T.-K., 2010, *Lg* attenuation in a region with both continental and oceanic environments, *Bulletin of the Seismological Society of America*, **100**, 851-858.
- Hong, T.-K., and Choi, H.-S., 2012, Seismological constraints on the collision belt between the North and South China blocks in the Yellow Sea, *Tectonophysics*, **570-571**, 102-113.
- Jun, M.-S., 1991, Body wave analysis for shallow intraplate earthquakes in the Korean Peninsula and Yellow Sea, *Tectonophysics*, **192**, 345-357.
- Jung, M.-K., and Kyung, J.-B., 2013, Source characteristics of the recent earthquakes for seven years in the southwestern region of the Korean Peninsula, *Journal of the Korean Earth Science Society*, **34**, 59-68.
- Jun, M.-S., and Jeon, J.-S., 2010, Focal mechanism in and around the Korean Peninsula, *Jigu-Mulli-wa-Mulli-Tamsa*, **13**, 198-202.
- Kim, S.-G., and Lee, S.-K., 2000, Seismic risk map of Korea obtained by using south and north Korea earthquake

- catalogues, *Journal of the Earthquake Engineering Society of Korea*, **4**, 13-34.
- Kim, S.-K., Jun, M.-S., and Jeon, J.-S., 2006, Recent research for the seismic activities and crustal velocity structure, *Economic and Environmental Geology*, **39**, 369-384.
- Kim, W.-H., Hong, T.-K., and Kang, T.-S., 2014, Hypocentral parameter inversion for regions with poorly known velocity structures, *Tectonophysics*, **627**, 182-192.
- Korea Institute of Geoscience and Mineral Resources, 1995, Geological Map of Korea.
- Korea Meteorological Administration, 2012, Historical earthquake records in Korean Peninsula.
- Kyung, J.-B., Cheong, T.-W., Lee, J.-G., Lee, D.-K., and Lee, E.A., 2001, Analysis of fault plane solution and stress field using the micro-earthquakes in the central region of South Korea, *Journal of the Korean Earth Science Society*, **22**, 292-300.
- Lee, M.-J., Kyung, J.-B., and Chi, H.-C., 2014, Fault plane solutions of the recent earthquakes in the northern part of the Korean Peninsula, *Journal of the Korean Earth Science Society*, **35**, 354-361.

- Paek, R.-J., Kang, H.-G., and Jon, G.-P., 1996, *Geology of Korea*, Foreign Languages Books Publishing House, Pyongyang, 631 p.
- Park, J.-C., Kim, W.-H., Chung, T.-W., Baag, C.-E., and Ree, J.-H., 2007, Focal mechanisms of recent earthquakes in the southern Korean Peninsula, *Geophysical Journal International*, **169**, 1103-1114.
- Park, J.-C., 2013, Characteristics of microseismicity in the southeastern area of the Korean Peninsula, *Thesis for an Master of Science Degree*, Pukyong National University, 66 p.
- Park, S.-C., Kong M.-K., Park, E.-H., Yun, W.-Y., and Hahm I.-K., 2012, Source parameters of the 2011 Yellow Sea earthquake ( $M_L$  5.3): Different features from earthquakes on the Korean Peninsula, *Earth Planets Space*, **64**, 379-388.
- Rhie, J.-K., and Kim, S.-R., 2010, Regional moment tensor determination in the southern Korean Peninsula, *Geosciences Journal*, **14**, 329-333.
- Snoke, J.-A., 2002, FOCMEC: focal mechanism determinations, in Lee, W. H. K., Jennings, P., Kisslinger, C., and Kanamori, H., ed., *International Handbook of Earthquake & Engineering Seismology*, Part B, Academic Press, San Diego, 1629-1630.

| No.      | KMA              |           |           |          |      | KIGAM       |          |          |            |      |
|----------|------------------|-----------|-----------|----------|------|-------------|----------|----------|------------|------|
|          | Origin time(KST) |           | Epicenter |          | Mag. | Epicenter   |          | Mag.     | Depth (km) |      |
| yy/mm/dd | hh:mm:ss         | Lat. (°N) | Lon. (°E) | hh:mm:ss |      | Lat.(°N)    | Lon.(°E) |          |            |      |
| 1        | 2016/08/18       | 22:21:10  | 38.84     | 125.70   | 2.6  | 22:21:11.13 | 38.8475  | 125.7069 | 2.7        | 6.2  |
| 2        | 2016/07/09       | 13:16:48  | 38.69     | 125.83   | 2.6  | 13:16:48.28 | 38.7693  | 125.8960 | 2.6        | 4.5  |
| 3        | 2016/06/25       | 03:24:52  | 38.74     | 125.86   | 2.6  | 03:24:52.47 | 38.8168  | 125.8849 | 2.7        | 11.3 |
| 4        | 2016/03/14       | 05:17:05  | 38.71     | 125.87   | 3.1  | 05:17:04.94 | 38.7824  | 125.8847 | 3.3        | 13.7 |
| 5        | 2016/02/28       | 16:52:38  | 38.73     | 125.85   | 2.5  | 16:52:38.15 | 38.7826  | 125.8913 | 2.6        | 13.7 |
| 6        | 2016/01/23       | 07:14:01  | 38.42     | 126.25   | 2.4  | 07:14:02.26 | 38.4091  | 126.2781 | 2.6        | 10.9 |
| 7        | 2015/01/06       | 13:06:40  | 38.43     | 126.28   | 2.8  | 13:06:40.72 | 38.4267  | 126.2709 | 2.9        | 13.4 |
| 8        | 2014/11/15       | 03:31:39  | 38.77     | 126.36   | 2.5  | 03:31:38.52 | 38.7852  | 126.3064 | 2.8        | 13.9 |
| 9        | 2014/06/21       | 08:29:30  | 38.77     | 125.89   | 2.6  | 08:29:30.78 | 38.8153  | 125.8937 | 2.9        | 4.0  |
| 10       | 2013/12/04       | 06:28:06  | 38.71     | 125.69   | 2.4  | 06:28:06.55 | 38.7198  | 125.6708 | 2.4        | 12.8 |
| 11       | 2013/12/02       | 20:02:58  | 38.56     | 126.10   | 2.8  | 20:02:58.32 | 38.5564  | 126.0879 | 2.8        | 12.5 |

|    |            |          |       |        |     |             |         |          |     |      |
|----|------------|----------|-------|--------|-----|-------------|---------|----------|-----|------|
| 12 | 2013/11/20 | 21:07:11 | 38.47 | 126.17 | 2.1 | 21:07:11.12 | 38.4602 | 126.1793 | 2.3 | 10.0 |
| 13 | 2013/11/16 | 22:32:45 | 38.51 | 125.66 | 2.1 | 22:32:45.50 | 38.5363 | 125.6694 | 2.4 | 11.9 |
| 14 | 2013/08/11 | 04:19:36 | 38.48 | 126.13 | 2.3 | 04:19:37.53 | 38.4368 | 126.1684 | 2.3 | 13.1 |
| 15 | 2013/07/01 | 11:24:54 | 38.78 | 126.36 | 3.0 | 11:24:54.83 | 38.7940 | 126.3203 | 3.2 | 12.6 |
| 16 | 2012/06/12 | 09:01:26 | 38.77 | 125.72 | 2.1 | 09:01:24.85 | 38.8179 | 125.6895 | 2.2 | -    |
| 17 | 2012/01/19 | 15:43:00 | 38.51 | 126.23 | 2.7 | 15:42:59.72 | 38.5437 | 126.2028 | 2.9 | 7.2  |
| 18 | 2011/09/28 | 13:20:04 | 38.48 | 126.26 | 2.6 | 13:20:04.37 | 38.4767 | 126.2825 | 2.8 | 13.3 |
| 19 | 2011/09/08 | 01:56:40 | 38.82 | 126.00 | 3.2 | 01:56:37.88 | 38.8795 | 125.9678 | 3.2 | 15.0 |
| 20 | 2011/08/15 | 06:10:40 | 38.47 | 125.63 | 3.2 | 06:10:40.00 | 38.5201 | 125.6541 | 3.5 | 13.3 |
| 21 | 2011/07/05 | 02:13:28 | 38.58 | 126.36 | 2.3 | 02:13:28.39 | 38.5763 | 126.3479 | 2.5 | 12.4 |
| 22 | 2011/03/06 | 11:04:39 | 38.66 | 125.67 | 2.9 | 11:04:39.48 | 38.7293 | 125.6782 | 2.9 | 10.8 |
| 23 | 2010/08/24 | 03:59:44 | 38.71 | 125.90 | 2.5 | 03:59:44.65 | 38.7695 | 125.9279 | 2.6 | 9.9  |
| 24 | 2010/06/22 | 22:21:02 | 38.46 | 125.64 | 2.6 | 22:21:02.41 | 38.4415 | 125.6442 | 2.5 | 15.4 |
| 25 | 2010/06/11 | 13:02:08 | 38.78 | 126.07 | 2.1 |             |         | No data  |     |      |
| 26 | 2010/04/16 | 19:56:11 | 38.78 | 126.01 | 2.2 | 19:56:11.73 | 38.8212 | 126.0041 | 2.4 | 7.2  |

|    |            |          |       |        |     |             |         |          |     |      |
|----|------------|----------|-------|--------|-----|-------------|---------|----------|-----|------|
| 27 | 2009/07/17 | 13:14:05 | 38.45 | 126.15 | 2.5 | 13:14:05.61 | 38.4549 | 126.1763 | 2.7 | 11.9 |
| 28 | 2009/06/03 | 20:09:38 | 38.57 | 126.50 | 2.9 | 20:09:38.38 | 38.5926 | 126.4898 | 3.0 | 15.0 |
| 29 | 2009/04/14 | 04:51:33 | 38.45 | 125.65 | 2.5 | 04:51:33.21 | 38.5043 | 125.6598 | 2.5 | 7.4  |
| 30 | 2008/11/11 | 23:37:54 | 38.56 | 125.66 | 2.5 | 23:37:56.68 | 38.4893 | 125.6639 | 2.8 | 12.0 |
| 31 | 2008/11/11 | 21:30:02 | 38.55 | 125.67 | 3.0 | 21:30:03.64 | 38.5201 | 125.6632 | 3.3 | 11.2 |
| 32 | 2008/11/11 | 21:20:53 | 38.54 | 125.65 | 3.0 | 21:20:54.65 | 38.5123 | 125.6598 | 3.4 | 13.5 |
| 33 | 2008/03/09 | 18:07:10 | 38.75 | 125.84 | 2.2 | 18:07:10.87 | 38.7923 | 125.8577 | 2.3 | 15.7 |

**Table 1.** Source parameters of the 33 earthquakes from KMA and KIGAM catalogs.

| No. | This study       |              |            |             |           |        |
|-----|------------------|--------------|------------|-------------|-----------|--------|
|     | Origin time(KST) |              | Epicenter  |             | Depth(km) | RMS    |
|     | yyyy/mm/dd       | hh:mm:ss     | Lat.(°N)   | Lon(°E)     |           |        |
| 1   | 2016-08-18       | 22:21:10.244 | 38.8237178 | 125.7136630 | 15.00     | 0.0541 |
| 2   | 2016-07-09       | 13:16:48.203 | 38.7036772 | 125.8453217 | 6.36      | 0.0287 |
| 3   | 2016-06-25       | 03:24:52.654 | 38.8978697 | 125.8950045 | 13.74     | 0.0702 |
| 4   | 2016-03-14       | 05:17:04.157 | 38.8261152 | 125.7982753 | 15.00     | 0.0232 |
| 5   | 2016-02-28       | 16:52:39.656 | 38.6435579 | 125.9151808 | 15.00     | 0.0763 |
| 6   | 2016-01-23       | 07:14:02.815 | 38.4762899 | 126.3184216 | 11.28     | 0.0315 |
| 7   | 2015-01-06       | 13:06:39.443 | 38.4724650 | 126.2602284 | 13.66     | 0.0157 |
| 8   | 2014-11-15       | 03:31:38.138 | 38.7346146 | 126.3070152 | 4.94      | 0.0119 |
| 9   | 2014-06-21       | 08:29:30.849 | 38.7870000 | 125.9406000 | 13.40     | 0.0337 |
| 10  | 2013-12-04       | 06:28:05.889 | 38.7233000 | 125.6246000 | 13.15     | 0.0247 |
| 11  | 2013-12-02       | 20:02:57.788 | 38.5984035 | 126.0820697 | 6.00      | 0.0106 |

|    |            |              |            |             |       |        |
|----|------------|--------------|------------|-------------|-------|--------|
| 12 | 2013-11-20 | 09:07:09.840 | 38.5005235 | 126.1682667 | 8.96  | 0.0009 |
| 13 | 2013-11-16 | 22:32:45.429 | 38.5906683 | 125.7262442 | 12.78 | 0.0427 |
| 14 | 2013-08-11 | 04:19:37.037 | 38.4802754 | 126.1294029 | 7.04  | 0.0732 |
| 15 | 2013-07-01 | 11:24:54.031 | 38.7287610 | 126.2907183 | 5.69  | 0.0015 |
| 16 | 2012-06-12 | 09:01:24.512 | 38.7055862 | 125.6238050 | 11.18 | 0.0946 |
| 17 | 2012-01-19 | 15:42:58.591 | 38.5523816 | 126.2118433 | 6.94  | 0.0152 |
| 18 | 2011-09-28 | 13:20:03.816 | 38.4916169 | 126.2967972 | 11.59 | 0.0146 |
| 19 | 2011-09-08 | 01:56:38.684 | 38.9103484 | 125.9834554 | 13.52 | 0.0326 |
| 20 | 2011-08-15 | 06:10:40.610 | 38.5571184 | 125.6287227 | 15.34 | 0.0097 |
| 21 | 2011-07-05 | 02:13:28.333 | 38.5904634 | 126.3316585 | 14.87 | 0.0386 |
| 22 | 2011-03-06 | 11:04:39.365 | 38.7303047 | 125.6679690 | 11.23 | 0.0209 |
| 23 | 2010-08-24 | 03:59:44.042 | 38.8325492 | 125.9451927 | 14.91 | 0.0169 |
| 24 | 2010-06-22 | 22:21:02.326 | 38.4103581 | 125.6496231 | 3.79  | 0.0012 |
| 25 | 2010-06-11 | 13:02:08.274 | 38.6897982 | 126.1241437 | 15.00 | 0.0655 |

|    |            |              |            |             |       |        |
|----|------------|--------------|------------|-------------|-------|--------|
| 26 | 2010-04-16 | 19:56:11.029 | 38.8743056 | 126.0431240 | 14.03 | 0.015  |
| 27 | 2009-07-17 | 13:14:05.746 | 38.4216621 | 126.2246977 | 11.48 | 0.0171 |
| 28 | 2009-06-03 | 20:09:37.487 | 38.6293203 | 126.4501486 | 7.03  | 0.0005 |
| 29 | 2009-04-14 | 04:51:33.512 | 38.5229367 | 125.5941620 | 9.08  | 0.0641 |
| 30 | 2008-11-11 | 23:37:55.889 | 38.5063701 | 125.5414466 | 15.00 | 0.0013 |
| 31 | 2008-11-11 | 21:30:04.439 | 38.5408694 | 125.7935625 | 7.98  | 0.0728 |
| 32 | 2008-11-11 | 21:20:54.344 | 38.4248996 | 125.8046137 | 5.11  | 0.0142 |
| 33 | 2008-03-09 | 18:07:08.888 | 38.7850000 | 125.7388000 | 15.00 | 0.0007 |

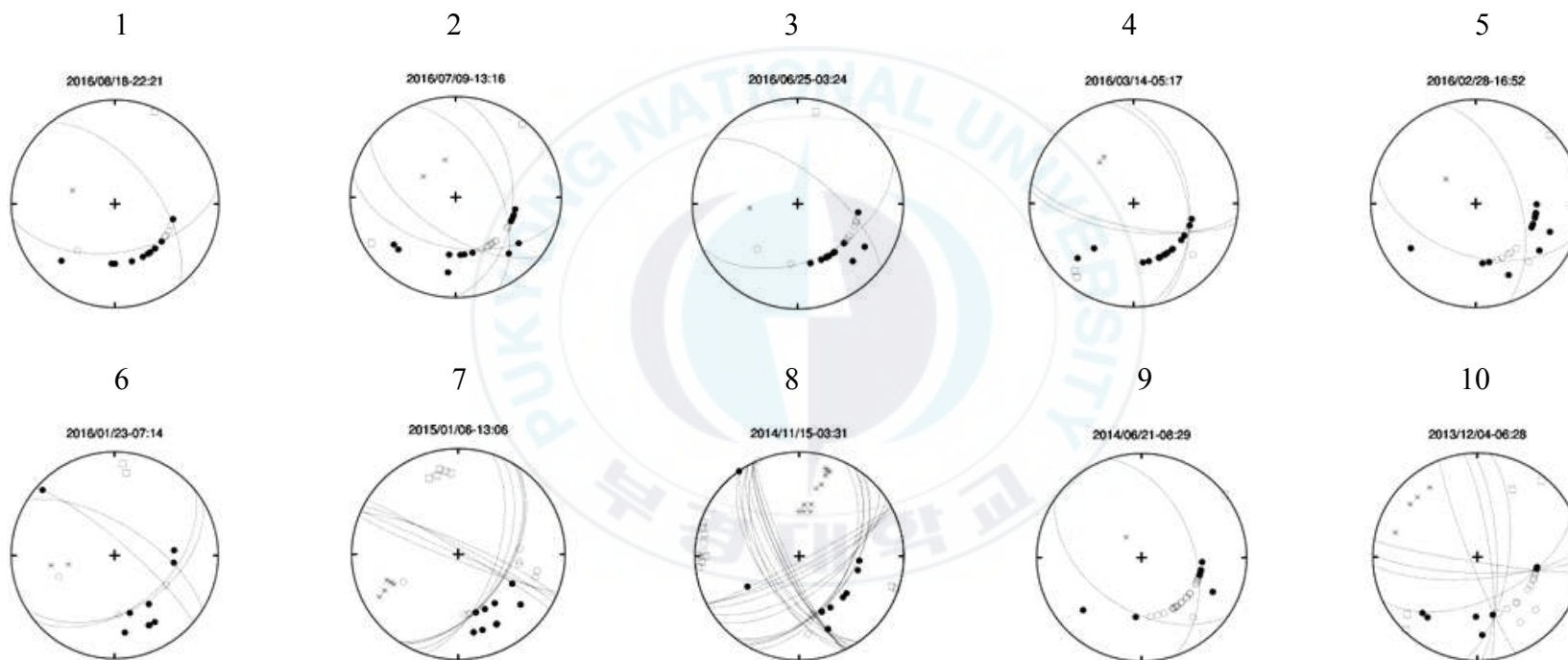
**Table 2.** Relocated hypocenters of 33 events in this study.

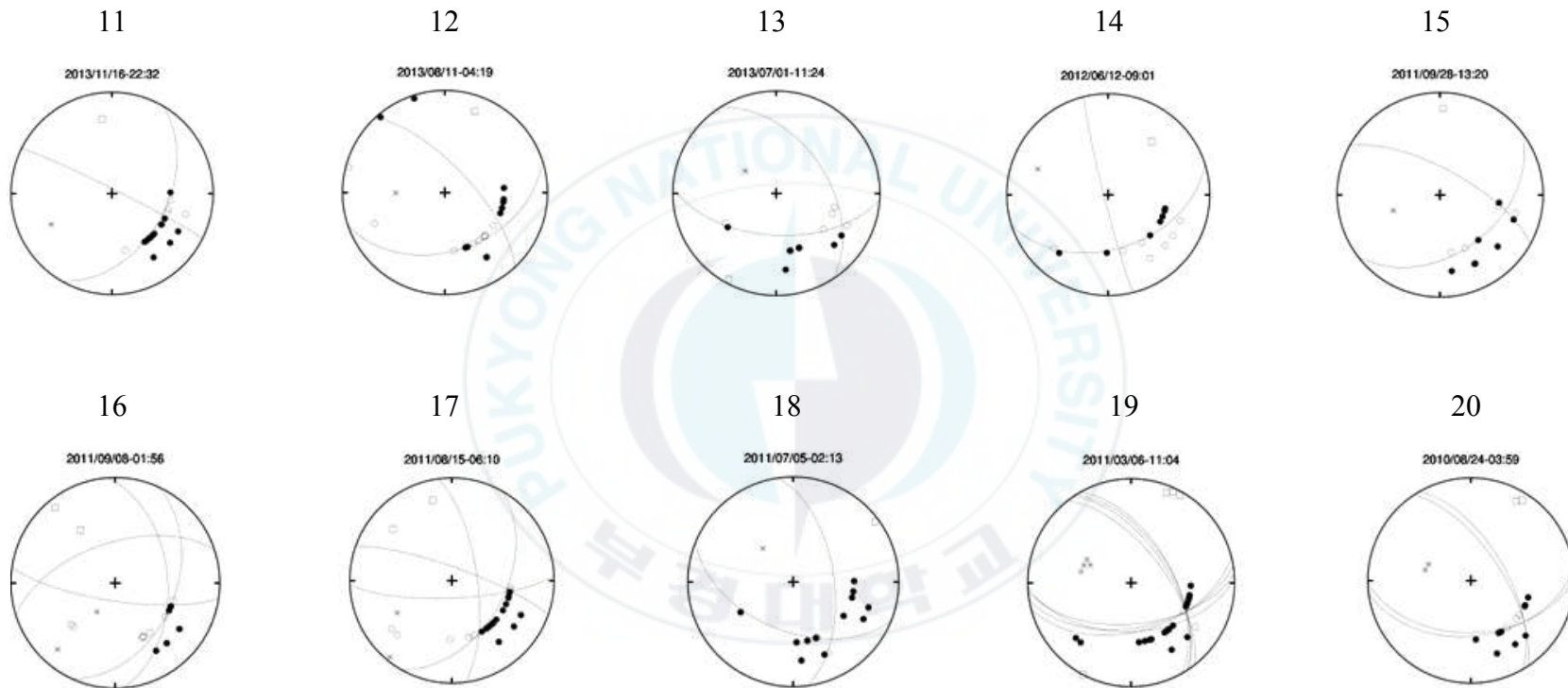
| This study |                           |       |        |        |       |        |         |
|------------|---------------------------|-------|--------|--------|-------|--------|---------|
| No.        | Origin time<br>yyyy/mm/dd | Dip   | Strike | Rake   | Dip   | Strike | Rake    |
| 1          | 2016/08/18                | 58.23 | 321.63 | -47.57 | 51.13 | 81.58  | -137.45 |
| 2          | 2016/07/09                | 56.17 | 336.31 | -53.00 | 48.44 | 102.76 | -131.93 |
| 3          | 2016/06/25                | 65.82 | 308.15 | -51.04 | 44.81 | 65.02  | -144.47 |
| 4          | 2016/03/14                | 48.44 | 345.89 | -30.79 | 67.48 | 97.46  | -134.1  |
| 5          | 2016/02/28                | 56.17 | 342.12 | -53.00 | 48.44 | 108.57 | -131.93 |
| 6          | 2016/01/23                | 65.82 | 302.05 | -51.04 | 44.81 | 58.92  | -144.47 |
| 7          | 2015/01/06                | 83.59 | 297.26 | -39.57 | 50.73 | 32.53  | -171.71 |
| 8          | 2014/11/15                | 60.22 | 50.43  | -19.3  | 73.33 | 150.3  | -148.77 |
| 9          | 2014/06/21                | 48.36 | 341.82 | -62.76 | 48.36 | 124.06 | -117.24 |
| 10         | 2013/12/04                | 74.81 | 357.84 | -13.17 | 77.30 | 91.34  | -164.42 |
| 11         | 2013/11/16                | 86.47 | 296.48 | -44.89 | 45.22 | 29.99  | -175.02 |
| 12         | 2013/08/11                | 69.75 | 317.01 | -52.31 | 42.06 | 71.14  | -148.89 |
| 13         | 2013/07/01                | 48.44 | 326.92 | -48.07 | 56.17 | 93.37  | -127.00 |
| 14         | 2012/06/12                | 86.47 | 165.87 | 44.89  | 45.22 | 72.36  | 175.02  |
| 15         | 2011/09/28                | 69.75 | 298.7  | -52.31 | 42.06 | 52.84  | -148.89 |
| 16         | 2011/09/08                | 76.00 | 98.51  | 43.22  | 48.36 | 355.7  | 161.12  |
| 17         | 2011/08/15                | 75.97 | 87.6   | 20.91  | 69.75 | 352.31 | 165.03  |
| 18         | 2011/07/05                | 58.23 | 352.14 | -47.57 | 51.13 | 112.09 | -137.45 |
| 19         | 2011/03/06                | 60.50 | 326.16 | -42.39 | 54.07 | 80.36  | -142.55 |

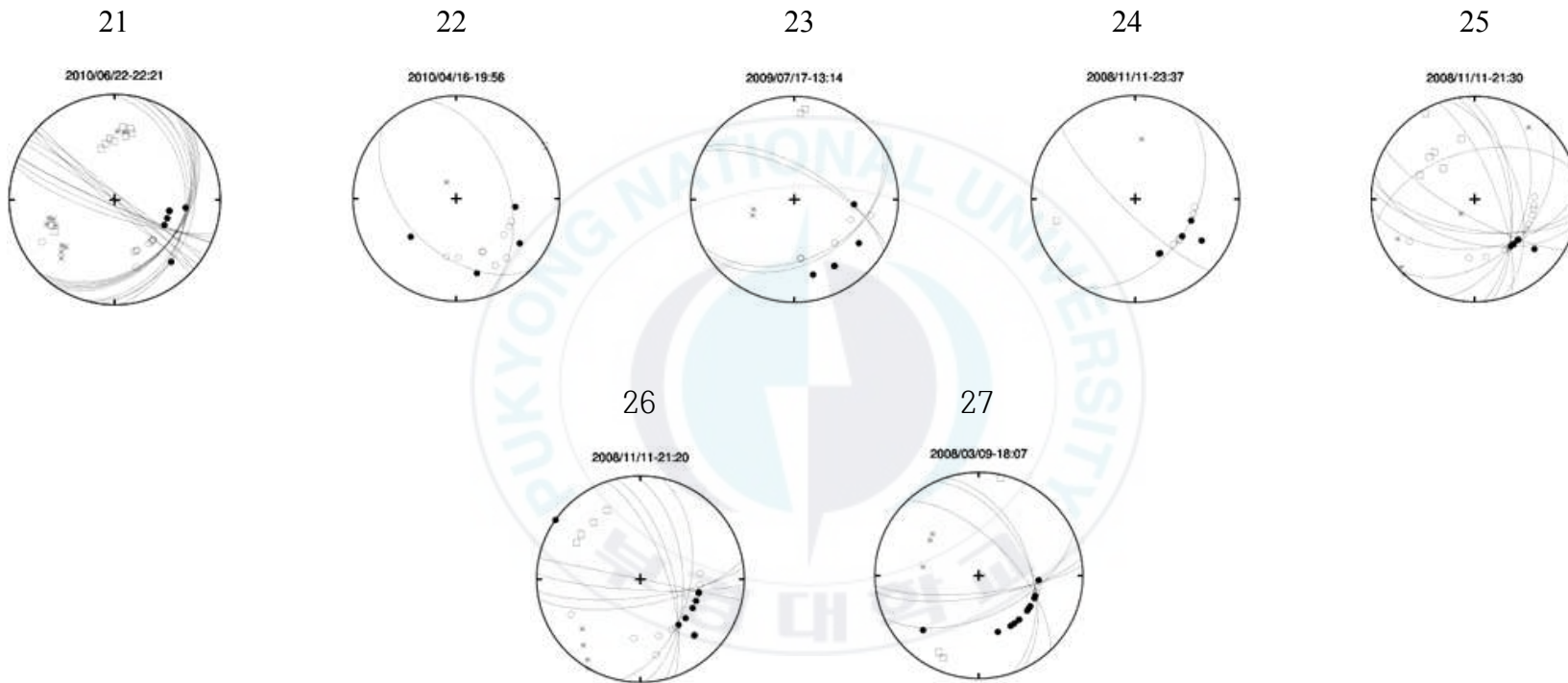
|    |            |       |        |        |       |        |         |
|----|------------|-------|--------|--------|-------|--------|---------|
| 20 | 2010/08/24 | 65.82 | 326.46 | -51.04 | 44.81 | 83.32  | -144.47 |
| 21 | 2010/06/22 | 90.00 | 122.03 | 55.00  | 35.31 | 40.71  | -172.90 |
| 22 | 2010/04/16 | 46.92 | 343.65 | -69.25 | 46.92 | 134.63 | -110.75 |
| 23 | 2009/07/17 | 68.53 | 297.64 | -57.5  | 38.29 | 57.52  | -143.8  |
| 24 | 2008/11/11 | 42.27 | 31.37  | -17.14 | 78.56 | 134.23 | -130.98 |
| 25 | 2008/11/11 | 65.60 | 100.31 | 32.73  | 60.5  | 355.44 | 151.66  |
| 26 | 2008/11/11 | 81.46 | 92.99  | 34.07  | 56.36 | 357.25 | 169.73  |
| 27 | 2008/03/09 | 50.14 | 335.42 | -22.91 | 72.61 | 80.57  | -137.81 |

**Table 3.** Parameters of fault plane solutions for 27 earthquakes that are analyzed using the seismic polarity analysis.

# Appendix







Appendix A. Focal mechanism solutions of 27 events.

# 한반도 평남분지의 지진 활동도

이 희 경

부경대학교 대학원 지구환경시스템과학과

## 요약

본 연구 지역은 한반도 북서부에 위치하고 지질학적으로 평남분지에 속하며 한반도 북부의 다른 지역에 비해 지진의 활동도가 비교적 높은 지역이다. 1982년 2월 14일, 중규모 지진이 황해북도 사리원 지역에서 발생했고, 이후 규모 4.0이하의 지진이 꾸준히 발생하고 있다. 본 연구에서는 2008년 3월부터 2016년 8월까지 황해북도 지역에서 발생한 33개의 지진을 분석하였다. 각 관측소에서 기록된 지진파 주행 시간의 오차가 최소화되는 지점을 결정할 때까지 반복적으로 계산하는 알고리즘을 사용하여 위치를 재결정하였고, 대부분의 지진들이 10~15km 깊이에서 발생한 것으로 추정되었다. 초동 극성법을 이용하여 대다수의 지진이 정단층 성분을 포함하는 주향이동단층과 관련이 있는 것으로 분석되었다. 지역적으로 perturbation이 일어났을 것으로 추정하나, 물리학적인 배경이 불확실하여 정확한 원인을 밝히는데 어려움이 있다. 과거 지진 활동도와 지진원을 분석하고, 지진 발생 메커니즘을 이해하며, 주된 응력의 방향을 분석하여 본 연구 지역에서 발생한 지진의 특성과 한반도 및 인근지역의 지체구조를 이해하는데 도움이 되고자 한다.